Using Near-Field Scan to Predict the Conducted Immunity of Electronic Components up to 6 GHz

Nicolas Castagnet, Alexandre Boyer, Fabien Escudié

Using Near-Field Scan to Predict the Conducted Immunity of Electronic Components up to 6 GHz

N. Castagnet[#*1], A. Boyer[*2], F. Escudié[#3]
[#]CEA, DAM, CEA-Gramat, F-46500 Gramat, France
[*]CNRS, LAAS, F-31400 Toulouse, France
{[1]nicolas.castagnet, [3]fabien.escudie}@cea.fr, [2]alexandre.boyer@laas.fr

***Abstract* — In the context of the growing threat of radio frequency directed energy weapons (RF DEW), near-field scan immunity (NFSI) stands as a powerful method for analysing the electromagnetic (EM) susceptibility of components, allowing the study of the response of an electronic device subject to an intentional electromagnetic interference (IEMI). This non-intrusive technique precisely targets component pins that are otherwise inaccessible with commonly used immunity investigation methods. In this paper, the quantitative measurement of the near-field coupling on a microstrip line is discussed and compared to a conducted injection based on the direct power injection (DPI) standard. Two E-field and H-field injection probes are calibrated and an experimental validation is conducted with both linear and non-linear loads. The results underscore the importance of NFSI in investigating systems vulnerability to RF DEW.**

***Keywords* — radio frequency directed energy weapons (RF DEW), intentional electromagnetic interference (IEMI), near-field scan immunity (NFSI), direct power injection (DPI), calibration.**

I. Introduction

In modern electronic systems, sophisticated and compact electronic components are increasingly used and potentially more vulnerable to failure in case of an IEMI. While the DPI method is commonly employed for precise analysis of integrated circuits (ICs) [1], it is highly intrusive, requiring the presence of a radio frequency (RF) connector mounted on the tested board, and it does not consider the real EM environment in which the component operates. Improving the investigation methodology is essential for enhancing the expertise in evaluating the vulnerability of systems to RF DEW.

In contrast, the near-field (NF) scan, as outlined in its IEC technical specification [2], provides a non-intrusive method to target component pins and diagnose EM susceptibility without altering the system's design. As the aggression is injected into the device under test (DUT) without direct contact, the coupling of the disturbance is different from that appearing in the case of a conducted injection. Therefore, the link between failure thresholds measured in conducted and near-field injections is not straightforward and a calibration process is required to quantify the electric (E) and magnetic (H) field produced by the injection probe and coupled onto the DUT. This versatile method can be used in various NF-based applications such as contactless current measurement [3], investigation of radiated immunity [4] and susceptibility of electronic devices to IEMI [5].

This paper introduces a new methodology for estimating conducted voltage on a DUT based on the amplitude injected with a near-field probe. An initial experimental approach is proposed in [6]. The aim is to improve the methodology for higher frequencies. Section II outlines a calibration process using the electric and magnetic moment based on the probe's performance factor which provides the tangential H-field or normal E-field produced by the injection probe above the calibration structure based on [7], [8]. Measurement uncertainties due to the incorrect positioning of the probe are then discussed. Section IV presents the theoretical equivalence between conducted and NF injection methods. The experimental validation and correlation between these techniques are shown in the last section on passive loads.

II. Determining the Coupling Between the Injection Probe and a Microstrip Line

The calibration of a NF injection probe relies on the measurement of the response of a calibration structure to the coupling of the E- and H-field generated by the injection probe placed in closed proximity. Some methods proposed the use of a waveguide [9], passive probe with creative design [10] or Helmholtz coils [11] to generate a controlled homogeneous field. However, the fields produced by the injection probes are not homogeneous and none of the previous cited methods can precisely estimate both E- and H-fields.

Microstrip line is commonly used as a calibration structure for EMC diagnosis and susceptibility analysis. It constitutes a simple structure and a convenient choice up to several gigahertz, until the quasi-TEM propagation assumption is not valid anymore. This solution is also approved by standards [12]. Although this structure seems simple, determining near-field distribution is not straightforward and 3D electromagnetic simulation is usually preferred [13]. Because of the complexity of EM solvers, it requires a solid expertise to select the most appropriate and the adequate configuration to ensure the validity and the convergence of the results. Computing the electric and magnetic moment based on the probe's performance factor can provide a practical and simple solution to determine the tangential H-field and normal E-field produced by the injection probe above a microstrip line [8]. Such formulations avoid the recourse of complex 3D EM simulators and facilitates the calibration process.

A. Design of the Calibration Structure

A 20-mm-long microstrip line is designed on a 1.5-mm-thick substrate, with a relative permittivity ϵ_r of 4.5. The linewidth is adjusted to ensure 50-Ω matching (w = 3 mm). The copper thickness T equals 35 µm. The loss tangent stands at 0.02 at 1 GHz, which is a typical value for FR4 substrate. The calibration process is described in Fig. 1. The probe is placed precisely at the controlled position P_0 (x_0, y_0, z_0).

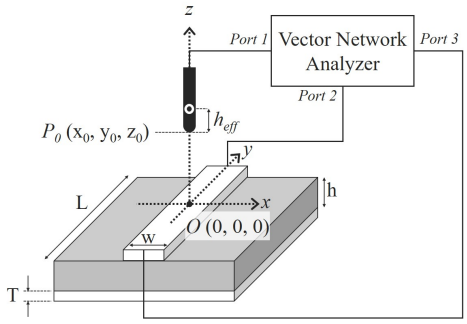

Fig. 1. Geometry of the microstrip line and probe's coordinates during calibration.

The experimental calibration process consists in measuring the transfer function (TF) between the probe and the calibration structure. It can be done using a vector network analyzer (VNA) connected to both line terminations and the probe. Furthermore, the probe has a negligible impact on the electric performance of the microstrip line. It is assumed that the probes behave like an elementary magnetic or electric dipole. As the injection probes are characterised only in the very-close reactive region of calibration, this assumption remains valid up to several gigahertz. The probe's position is set above the line centre, at $x_0 = y_0 = 0$ mm and $z_0 = 0.5$ mm.

B. Expression of the Transfer Function between the H-field Probe and the Calibration Structure

The probe sensitivity is given by its performance factor (PF) which is the ratio between the induced voltage at the probe tip and the incoming H-field. Assuming that the probe is represented as an elementary dipole, the effective height h_{eff} is also a significant parameter. It is the distance between the probe tip and the point where an ideal infinitesimal probe would provide the same result as mentioned in Fig. 1. The general PF for an H-field probe is given by (1), where V_{fwd} is the voltage of the forward wave produced at Port 1 of the VNA and $S_{21}(f)$ is the TF of the probe. Although all these quantities are complex, only the magnitude is considered here.

$$PF_H(f) = \frac{V_{fwd} \cdot S_{21}(f)}{H(x_0, y_0, z_0 + h_{eff}, f)} \tag{1}$$

The Langer SX-R 3-1 H-field probe has been selected for this paper. Its frequency range extends from 1 to 10 GHz. The PF of a single loop is generally expressed as (2), where μ_0 is the vacuum magnetic permeability and r_{loop} the inner radius of the loop.

$$PF_H(f) = \mu_0 \cdot 2\pi f \cdot r_{loop}^2 \tag{2}$$

Probe's head diameter is 3 mm and the PF at 1 GHz is -39 dB [14]. From (2), the value of r_{loop} is 0.67 mm and its accuracy has been verified through measurement. The injection probe is modelled by an equivalent magnetic dipole located at the probe's head centre (h_{eff} = 1.5 mm) and the magnetic moment m_H is calculated according to (3), where I stands for the probe excitation current As m_H varies according to the excitation current, it is given for a normalisation current equal to 1 A.

$$m_H = I \cdot \pi \cdot r_{loop}^2 = 1.41 \cdot 10^{-6} A/m^2 \tag{3}$$

The radiated immunity tool provided by the IC-EMC software [15] is employed to determine the voltage amplitude V_{mes} induced on a line termination based on calibration structure characteristics (see Section II-A), the probe placement and its equivalent magnetic moment m_H. The equation which defines the relationship between the simulated S_{21} and V_{mes} is given by (4).

$$S21_{sim} = \frac{V_{mes}}{V_{fwd}} = 2\frac{V_{mes}}{V_S} = 2\frac{V_{mes}}{Z_C \cdot I} \tag{4}$$

Subsequently, by setting Z_C to 50 Ω, the simulated TF is juxtaposed against the measured one in Fig. 2.

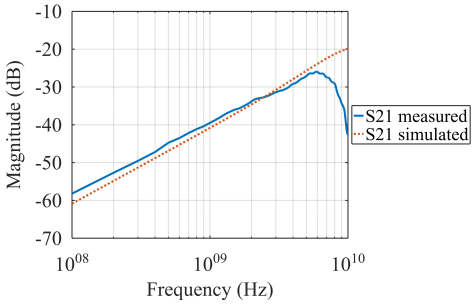

Fig. 2. Comparison between measured and simulated transfer functions of the H-field probe Langer SX-R 3-1.

A good agreement is observed between the measured and simulated TF up to 6 GHz with less than a 10% disparity. However, at higher frequencies, the quasi-TEM mode hypothesis is no longer valid and the microstrip line becomes dispersive. In this study, the magnetic moment is constant over frequency. Adjusting it based on calibration data from Langer could enhance the agreement at low frequencies.

These results prove the relevance of a calibration approach of the injection probe based on magnetic dipole assumption, at least up to 6 GHz.

C. Expression of the Transfer Function between the E-field Probe and the Calibration Structure

Compared with the H-field, the computation of the E-field coupled to the calibration structure is more challenging due to the air–dielectric interface and the ground plane leading to multiple reflections. In addition, the E-field coupling does not depend only on the probe head but also on the probe shielding and h_{eff} is not constant for small scan height [7].

The E-field probe used in this section is the Langer SX-E 03. The PF is not given by the manufacturer but extracted

from [7] and the electric moment m_E is defined in (5), where V_G is the RF generator amplitude, Z_C its output impedance (50 Ω), C the parasitic capacitance of the probe and V_{fwd} the forward voltage amplitude. As m_E depends on V_{fwd}, m_E is given for a normalisation V_{fwd} equal to 1 V.

$$m_E(f) = h_{eff}\frac{V_G}{Z_C + \frac{1}{jC\cdot 2\pi f}} = 2\frac{V_{fwd}}{Z_C}PF_E(f) \qquad (5)$$

By analysing the probe's geometry, h_{eff} is sets to 1.5 mm and for each frequency f_i, $m_E(f_i)$ is computed from $PF_E(f_i)$. Once again, the radiated immunity tool provided by the IC-EMC software is used to find V_{mes} and $S21_{sim}$ according to (4). Fig. 3 compares the measured and simulated transfer functions of the E-field probe.

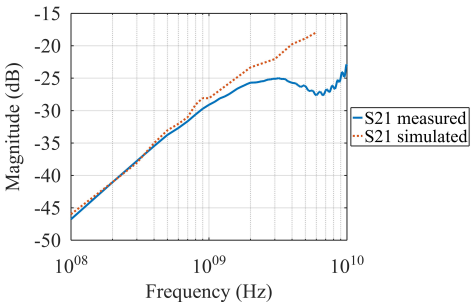

Fig. 3. Comparison between measured and simulated transfer functions of the E-field probe Langer SX-E 03.

The simulated TF of the E-field probe correlates to the measurements up to 1.5 GHz at less than 10 % difference. Uncertainty about the h_{eff} position of the centre of the electric dipole leads to significant divergence at high frequencies. Despite the assumptions and uncertainties, these first results are interesting and reinforces the need to calibrate the probes to accurately quantify the E- or H-field coupled onto a DUT.

III. Effects of a Misplaced Near-Field Probe

In this section, the effect of displacements of the probe relative to its initial calibration position is investigated. It is assumed that the length of the calibration structure's trace significantly exceeds the wavelength, ensuring consistent coupling regardless of the probe's position above the trace, as long as $x = 0$ and z remain constant. The effects of coupling at the board's boundaries are not addressed.

A. Shifting the NF Probes Along x-axis

The coordinates described here are those defined in Fig. 1. The height z is set to 0.5 mm and for $y = 0$, transfer functions $S21_E$ and $S21_H$ of the E- and H-field injection probes are measured for different values of x. Fig. 4 shows the average attenuation between 100 MHz and 10 GHz compared to the calibration point P_0 $(0, 0, 0.5)$ measured in Section II. The line width w is 3 mm and depicted by the dotted line.

Results show that the maximum variation of the coupling is -5 dB if the probe is positioned above the line. A typical positioning error of 200 µm results in a deviation of only 0.1 dB. The results align with findings from other studies [13].

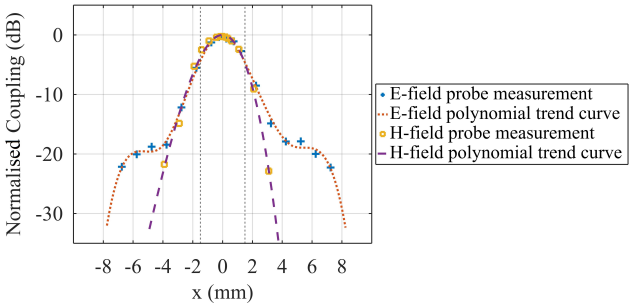

Fig. 4. Measured E- and H-field coupled to the microstrip line for various x values compared to the E- and H-field coupled at the calibration point P_0.

B. Shifting the NF Probes Along z-axis

E- and H-fields probes are centred in $x = y = 0$. Transfer functions $S21_E$ and $S21_H$ are measured for different heights and compared to the TF measured at the origin point O $(0, 0, 0)$ as described in Fig. 5.

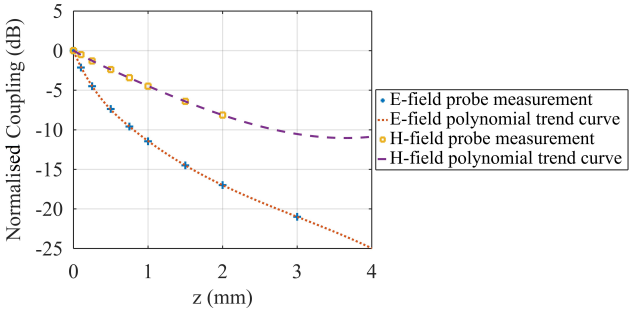

Fig. 5. Measured E- and H-field coupled to the microstrip line for various z values compared to the E- and H-field coupled at the origin point O.

For a calibration point set to $(0, 0, 0.5)$, incorrect positioning of 200 µm yields a difference of 1 dB and 2.5 dB for H-and E-field measurements respectively. Furthermore, experimental results agree with the theory that the dominant field component has an attenuation in $1/z^3$ in a very-close distance of the probe.

These results demonstrate that the transfer function measured at the calibration point can be reliably used with a 2-dB confidence level even if probes are displaced by 200 µm in z and x directions due to set-up uncertainties.

IV. Theoretical Equivalence Between Conducted and Near-Field Injections

A. Definition of the Electromagnetic Susceptibility Measurement Methods

The objective of the DPI is to apply an RF disturbance to a pin of an IC to quantify the amplitude required for the occurrence of a failure (typically measured as the forward power captured through a bidirectional coupler and an RF power meter). As depicted in Fig. 6, the harmonic disturbance is generated by an RF signal generator and injected into the DUT through a bidirectional coupler and a high-pass filter (bias tee) that blocks the DC voltage.

The NFSI technique is based on the use of a miniature probe (with diameters ranging from hundreds of micrometres to millimetres) generating an H- or E-field near the DUT. The coupling of this field onto the DUT induces voltage fluctuations across the pins of the IC that may lead to component failure. In this study and as described in Fig. 7, it is assumed that the injection probe is located above a 50-Ω matched microstrip line, which is connected to the actual characteristic impedance Z_C of the system on one end and to the DUT on the other end.

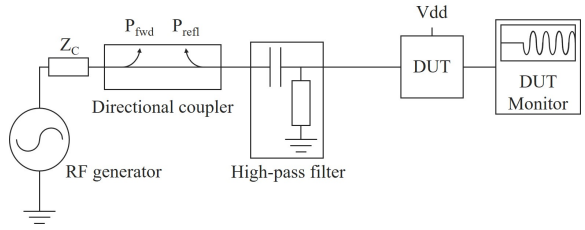

Fig. 6. Direct Power Injection set-up.

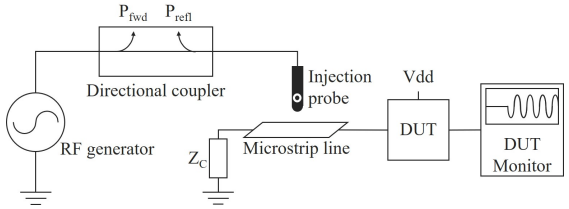

Fig. 7. Near-Field Injection set-up.

Modelling the DPI and NFSI set-ups involves characterising all the elements of the aggression paths with a VNA.

B. Equivalent Approach using Chained Matrices

The approach employed in this paper involves characterising all components of the aggression path using their respective S-parameter matrices. By chaining these matrices together (after subsequently converting them into ABCD matrices), we can determine the transmission coefficients S_{21}^{DPI} and S_{21}^{NFSI} between the RF generator and the DUT for each technique. It is assumed that a failure occurs at the DUT at a given frequency for an amplitude V_{DUT} applied to one pin of the component, represented by its impedance Z_{DUT}. Fig. 8 shows the equivalent schematic of the models of injection chain (DPI or NFSI) presented in the previous section as an S-parameters box. V_G and Z_G are respectively the equivalent amplitude and impedance of the RF generator.

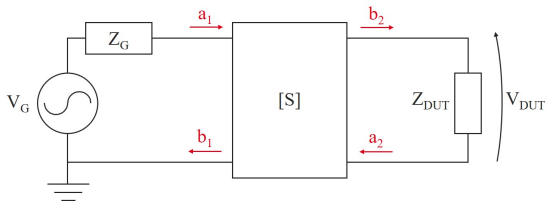

Fig. 8. Diagram of the aggression path with an S-parameters box.

Let Z_C be the real characteristic impedance of the line. The reflection coefficients of the load Γ_{DUT} and the source Γ_G are defined by (6) and (7).

$$\Gamma_{DUT} = \frac{Z_{DUT} - Z_C}{Z_{DUT} + Z_C} \tag{6}$$

$$\Gamma_G = \frac{Z_G - Z_C}{Z_G + Z_C} \tag{7}$$

The reflection coefficient ρ is seen from port 1 of the S-parameters box.

$$\rho = S_{11} + \frac{\Gamma_{DUT} S_{12} S_{21}}{1 - \Gamma_{DUT} S_{22}} \tag{8}$$

Knowing that $a_1 = \frac{V_G}{2} \cdot \frac{1-\Gamma_G}{1-\rho\Gamma_G}$, b_2 is defined as $b_2 = S_{21}\, a_1 + S_{22}\, a_2$ with $a_2 = \Gamma_{DUT}\, b_2$. So :

$$b_2 = \frac{V_G}{2} \cdot \frac{S_{21}(1-\Gamma_G)}{(1-\Gamma_G S_{11})(1-\Gamma_{DUT} S_{22}) - \Gamma_G \Gamma_{DUT} S_{12} S_{21}} \tag{9}$$

The voltage V_{DUT} applied across the component's pins is $V_{DUT} = b_2(1+\Gamma_{DUT})$. Combined with (9), the expression of the voltage to the DUT is given by (10).

$$V_{DUT} = \frac{V_G}{2} \cdot \frac{S_{21}(1-\Gamma_G)(1+\Gamma_{DUT})}{(1-\Gamma_G S_{11})(1-\Gamma_{DUT} S_{22}) - \Gamma_G \Gamma_{DUT} S_{12} S_{21}} \tag{10}$$

1) Specific case

An injection set-up must be designed with the most adapted components as possible. In a conducted injection test like the DPI, $Z_G = Z_C$ and $S_{11} = S_{22} = 0$. But this last statement is valid in NFSI only if the microstrip line is 50-Ω matched. In this case, (10) turns to (11).

$$V_{DUT} = \frac{V_G}{2} \cdot S_{21}(1+\Gamma_{DUT}) \tag{11}$$

If a failure occurs for an amplitude V_{DUT}^{DPI} during a DPI test, it also appears when the same voltage is applied to the component with a near-field probe. Thus, $V_{DUT}^{DPI} = V_{DUT}^{NFSI}$, leading to (12) and (13).

$$\frac{V_G^{DPI}}{2} \cdot S_{21}^{DPI}(1+\Gamma_{DUT}) = \frac{V_G^{NFSI}}{2} \cdot S_{21}^{NFSI}(1+\Gamma_{DUT}) \tag{12}$$

$$V_G^{DPI} S_{21}^{DPI} = V_G^{NFSI} S_{21}^{NFSI} \tag{13}$$

The relationship between the amplitude required in both set-ups for the appearance of the same failure is described in (13).

V. Validation of the Equivalence Method on Passives Loads

Due to the calibration results described in Section II, the frequency range extends from 1 to 6 GHz in steps of 100 MHz. S_{21}^{DPI} and $S_{21}^{NFSI}|_E$ and $S_{21}^{NFSI}|_H$ are extracted from the S-parameters of the aggression path (see Section IV-B) and the transfer functions of both injection probes. Correction functions K_E and K_H are employed to adjust the RF generator during NFSI tests in order to yield the same results as those

obtained with DPI. These functions are defined in (14) and (15) from (13).

$$K_E = \frac{S_{21}^{DPI}}{S_{21}^{NFSI}|_E} \tag{14}$$

$$K_H = \frac{S_{21}^{DPI}}{S_{21}^{NFSI}|_H} \tag{15}$$

Fig. 9 shows the measured transfer functions as well as the corrective ones.

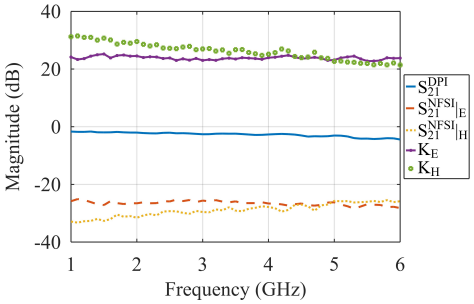

Fig. 9. Transfer functions of the two susceptibility measurement methods (DPI and NFSI) as a function of magnetic (H) or electric (E) coupling, along with K_E and K_H corrective functions.

The decrease of S_{21}^{DPI} is due to power losses in the agression path. The amplitude V_G^{DPI} of the continuous wave signal created by the RF generator during a conducted aggression is maintained constant for the entire frequency range under study. In contrast and as mentioned in (13), the source voltage for NFSI is changed according to the frequency and the type of coupling in order to induce the same level of voltage across the DUT.

A. Experimental Results on Real Impedances

An initial validation of the correlation between DPI and NFSI for both types of coupling (electric and magnetic) is performed on 51 Ω and 510 Ω SMD 0805 resistors from Vishay. Fig. 10 shows the amplitude in dBV measured with an oscilloscope.

A good agreement is observed for both near-field injection types, which validates the model established in this paper. The small variation between conducted and near-field injection results arises from the misplacement of the injection probe above the microstrip line as described in Section III and measurement uncertainties. The study has been conducted with five other resistors values yielding similar results.

B. Experimental Results on Complex Impedances

The same experiment has been repeated with complex impedances. Fig. 11 shows the amplitude in dBV measured across 100 pF and 10 µF MLCC capacitors.

These two simple case studies validate the near-field and conducted injection correlation model for H-field and E-field coupling on linear passive components.

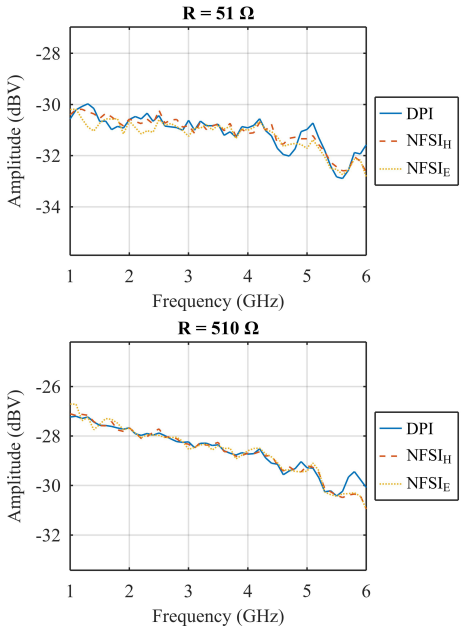

Fig. 10. Comparison of voltages across resistors for different injection techniques (DPI, NFSI with H-field and E-field probes).

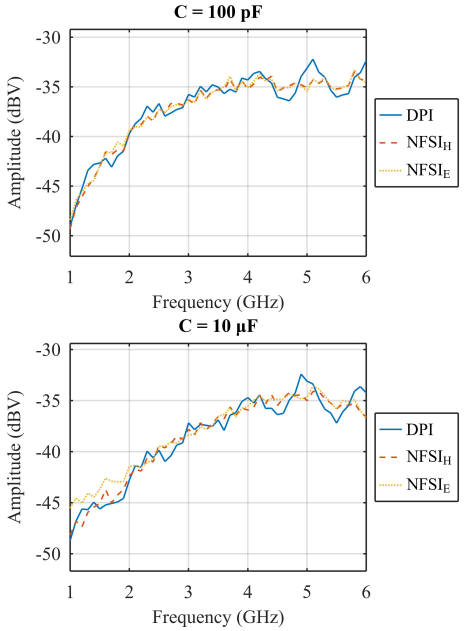

Fig. 11. Comparison of voltages across capacitors for different injection techniques (DPI, NFSI with H-field and E-field probes).

C. Experimental Results on a Non-linear Component

The methodology validation is now conducted using the Zener diode BZX55C 0v8, which has a Zener voltage of 0.8 V and is mounted in a DO-35 case. The anode is connected to the ground while the cathode is connected to the line. The reflection and transmission coefficients of the diode are illustrated in Fig. 12 for an excitation power of 0 dBm.

S-parameters of the diode remain constant regardless of the increase of the VNA power and it can be seen as a RLC multiresonant model in HF. The same experiment as in

Section V-A and V-B is performed and results are shown in Fig. 13.

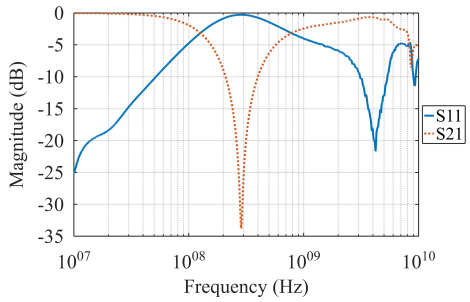

Fig. 12. Reflection coefficient $S11$ and transmission coefficient $S21$ of the Zener diode BZX55C 0v8 for an excitation power of 0 dBm.

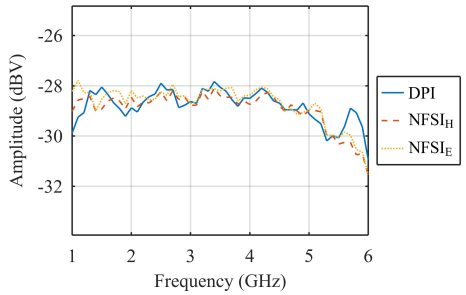

Fig. 13. Comparison of voltages across a Zener diode for different injection techniques (DPI, NFSI with H- and E-field probes).

Once again, a good agreement is observed for both near-field injection types in comparison to the DPI method. However, the RF disturbance's amplitude was insufficient to activate the diode. Overlaying a DC bias onto the signal should be an interesting improvement for exploring the diode's response when triggered.

VI. Conclusion

Near-Field Scan Immunity is a promising technique for investigating the vulnerability of electronic systems to an IEMI in a non-intrusive manner. Assumptions based on elementary dipole models for E- and H-field injection probes have yielded reliable results up to 1.5 GHz and 6 GHz respectively. A calibration process has been proposed and experimental results demonstrate that the calibration point can be reliably used with less than 2-dB confidence level even if the probes are displaced by 200 µm from the centre of the calibration structure. By quantitatively measuring the near-field coupling on a microstrip line, this approach has been compared to the conducted injection method with both linear and non-linear loads. An excellent agreement has been observed up to 6 GHz with minor variations.

Despite the challenges posed by the complexity of the EM fields and uncertainties in probe positioning, NFSI emerges as a powerful tool for evaluating the susceptibility of civil and military electronic devices to an RF DEW. Further work should extend the equivalence relationship between conducted and NF injection for unknown load impedances. The possibility of studying the calibration of the field generated by the probe independently of a coupling structure should also be considered. Furthermore, the E-field produced by the H-field probe and the H-field produced by the E-field probe should be investigated.

Acknowledgment

This work is financially supported by the French Ministry of Defense - Defense Innovation Agency.

References

[1] *Integrated Circuits, Measurement of Electromagnetic Immunity, 150 kHz to 1 GHz - Part 4: Direct RF power injection method*, International Electrotechnical Commission Std. IEC 62 132-4, 2014.

[2] *Integrated circuits, Measurement of electromagnetic immunity – Part 9: Measurement of radiated immunity – Surface scan method*, International Electrotechnical Commission Std. IEC TS 62 132-9, 2014.

[3] F. Caignet, N. Nolhier, and M. Bafleur, "Dynamic system level ESD current measurement using magnetic field probe," in *Asia–Pacific Symposium on Electromagnetic Compatibility (APEMC)*, Taipei, Taiwan, May 2015, pp. 490–493.

[4] A. Durier, S. B. Dhia, and T. Dubois, "Study of the radiated immunity of a drain-source current sensor using Near Field Scan Immunity method," in *12th International Workshop on the Electromagnetic Compatibility of Integrated Circuits (EMC Compo)*, Hangzhou, China, 2019, pp. 52–54.

[5] L. C. Lavau, M. Suhrke, and P. Knott, "Impact of IEMI pulses on a barometric sensor," in *2022 International Symposium on Electromagnetic Compatibility (EMC Europe)*, 2022, pp. 290–294.

[6] N. Castagnet, F. Escudié, and A. Boyer, "Modèle d'estimation de la susceptibilité conduite à partir d'une injection champ proche entre 500 MHz et 2 GHz," in *Dixième Conférence Plénière du GDR Ondes*, Marseille, France, Dec. 2023.

[7] A. Boyer, N. Nolhier, F. Caignet, and S. B. Dhia, "Closed-Form Expressions of Electric and Magnetic Near-Fields for the Calibration of Near-Field Probes," *IEEE Trans. Instrum. Meas.*, vol. 70, pp. 1–15, 2021.

[8] A. Boyer *et al.*, "On the Correlation Between Near-Field Scan Immunity and Radiated Immunity at Printed Circuit Board Level – Part I," *IEEE Electromagn. Compat.*, vol. 64, no. 4, p. 1230–1242, Aug. 2022.

[9] P. Payet, J. Raoult, and L. Chusseau, "Remote extinction of a 2.4 GHz RF front-end using millimeter-wave EMI in the near-field," *Progress in Electromagnetics Research Letters*, vol. 68, pp. 99–104, 2017.

[10] R. Adam, L. Chusseau, T. Grosjean, A. Penarier, J. Guilleta, and D. Charraut, "Near-field wire-based passive probe antenna for the selective detection of the longitudinal electric field at terahertz frequencies," *Journal of Applied Physics*, vol. 106, no. 7, p. 073107, Oct. 2009.

[11] Y. Zhao *et al.*, "Measurement of near-field electromagnetic emissions and characterization based on equivalent dipole model in time-domain," *IEEE Trans. Electromagn. Compat.*, vol. 62, no. 4, p. 1237–1246, Aug. 2020.

[12] *Integrated circuits, Measurement of electromagnetic emissions – Part 3: Measurement of radiated emissions – Surface scan method*, International Electrotechnical Commission Std. IEC TS 61 967-3, 2014.

[13] S. Jarrix, T. Dubois, R. Adam, P. Nouvel, B. Azais, and D. Gasquet, "Probe Characterization for Electromagnetic Near-Field Studies," *IEEE Trans. Instrum. Meas.*, vol. 59, no. 2, pp. 292–300, Feb. 2010.

[14] Langer EMV-Technik GmbH. SX-R 3-1 H-field probe (1 GHz up to 10 GHz). [Online]. Available: https://www.langer-emv.de/en/product/sx-passive-1ghz-up-to-20-ghz/33/sx-r-3-1-h-field-probe-1-ghz-up-to-10-ghz/

[15] IC-EMC website. [Online]. Available: http://www.ic-emc.org/